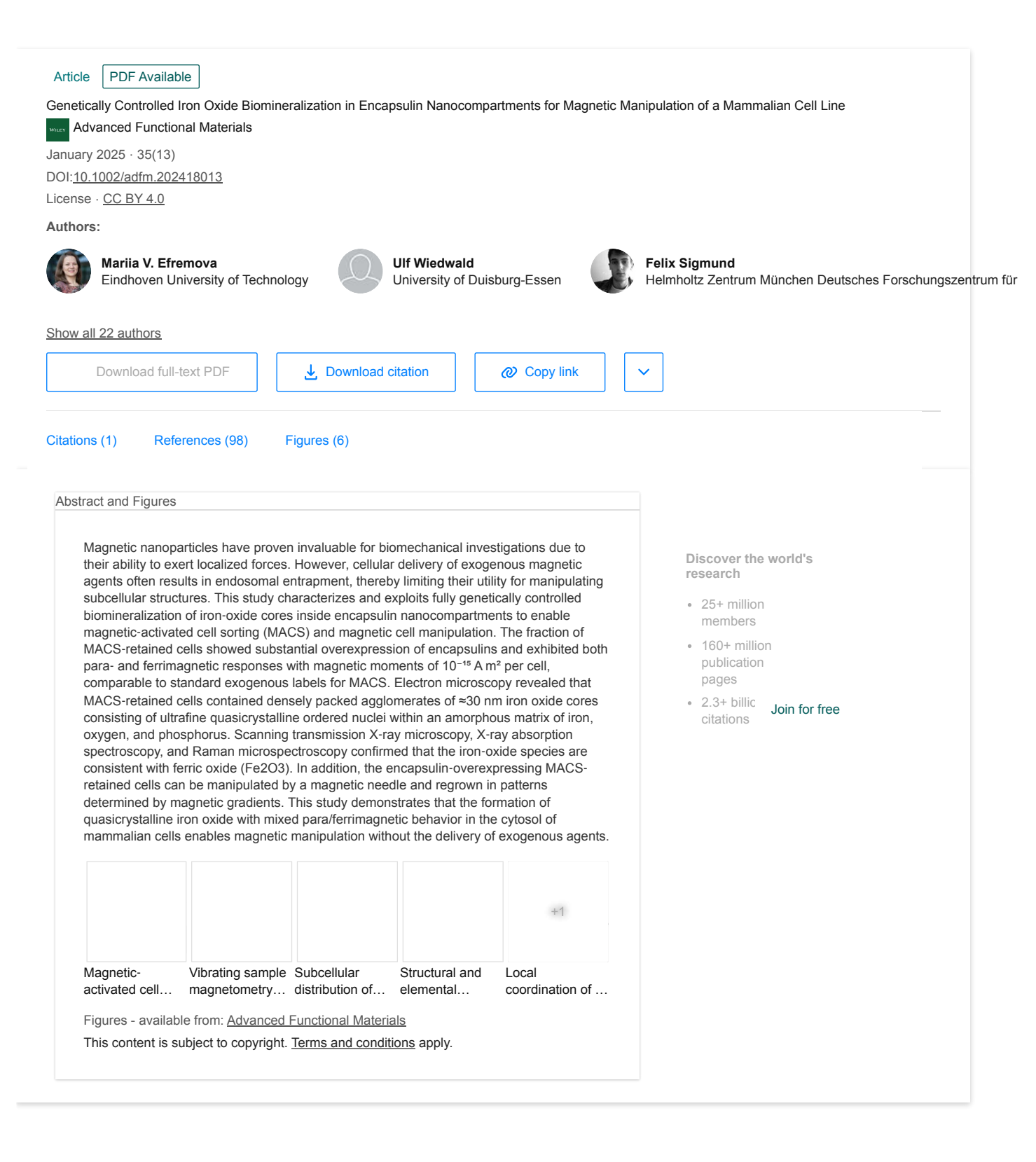
Recruit researchers Join for free Login



Publisher Full-text 1

Access to this full-text is provided by Wiley.

Learn more

Content available from Advanced Functional Materials This content is subject to copyright. Terms and conditions apply.

RESEARCH ARTICLE

www.afm-journal.c

Genetically Controlled Iron Oxide Biomineralization in Encapsulin Nanocompartments for Magnetic Manipulation of a Mammalian Cell Line

Maria V. Efremova,* Ulf Wiedwald, Felix Sigmund, Silviu-Vasile Bodea, Hendrik Ohldag, Thomas Feggeler, Ralf Meckenstock, Lorenz N. Panzl, Jeroen Francke, Irina Beer, Natalia P. Ivleva, Irina B. Alieva, Anastasiia S. Garanina, Alevtina S. Semkina, Franziska Curdt, Nicolas Josten, Sebastian Wintz, Michael Farle, Reinoud Lavrijsen, Maxim A. Abakumov, Michael Winklhofer, and Gil G. Westmeyer*

Magnetic nanoparticles have proven invaluable for biomechanical investigations due to their ability to exert localized forces. However, cellular delivery of exogenous magnetic agents often results in endosomal entrapment, thereby limiting their utility for manipulating subcellular structures. This study characterizes and exploits fully genetically controlled biomineralization of iron-oxide cores inside encapsulin nanocompartments to enable magnetic-activated cell sorting (MACS) and magnetic cell manipulation. The fraction of MACS-retained cells showed substantial overexpression of encapsulins and exhibited both para- and ferrimagnetic responses with magnetic moments of 10⁻¹⁵ A m² per cell, comparable to standard exogenous labels for MACS. Electron microscopy revealed that MACS-retained cells contained densely packed agglomerates of ≈30 nm iron oxide cores consisting of ultrafine quasicrystalline ordered nuclei within an amorphous matrix of iron, oxygen, and phosphorus. Scanning transmission X-ray microscopy, X-ray absorption spectroscopy, and Raman microspectroscopy confirmed that the iron-oxide species are consistent with ferric oxide (Fe₂O₃). In addition, the encapsulin-overexpressing MACS-retained cells can be manipulated by a magnetic needle and regrown in patterns determined by magnetic gradients. This study demonstrates that the formation of quasicrystalline iron oxide with mixed para/ferrimagnetic behavior in the cytosol of mammalian cells enables magnetic manipulation without the delivery of exogenous agents.

1. Introduction

The use of synthetic magnetic nan materials has a long history biomechanical studies of cells.\(^{1}

Fully genetic methods to generate bi magnetic structures would be desirabl but the only experimentally confirmed is stances of genetically controlled magnet materials in nature are found in so-calle magnetosomes inside magnetotact bacteria, [3–5] as extracellular iron biomin eralization products in the teeth (radula of certain mollusks and vertebrates, [6–as well as in candidate magnetorece tor structures of some vertebrates.]

Overexpression of ferritin, the mo abundant iron-storing protein complin mammalian cells, has been propose as a biomagnetic handle. Howeve calculations show that the magnet properties of native ferritin, which cotains the low-magnetization ferrihydri [FeO(OH)] $_8$ [FeO(H $_2$ PO $_4$)] are orders magnitude too weak to support the proposed mechanisms. However, the magnetical magnetical support the proposed mechanisms.

M. V. Efremova, F. Sigmund, S.-V. Bodea, L. N. Panzl, G. G. Westmeyer Department of Bioscience of TUM School of Natural Sciences and TUM School of Medicine and Health

Technical University of Munich Ismaninger Str. 22, 81675 Munich, Germany E-mail: m.efremova@tue.nl; gil.westmeyer@tum.de

The ORCID identification number(s) for the author(s) of this article can be found under https://doi.org/10.1002/adfm.202418013

© 2025 The Author(s). Advanced Functional Materials published by Wiley-VCH GmbH. This is an open access article under the terms of the Creative Commons Attribution License, which permits use, distribution and reproduction in any medium, provided the original work is properly cited.

DOI: 10.1002/adfm.202418013

M. V. Efremova, F. Sigmund, S.-V. Bodea, L. N. Panzl, G. G. Westmeyer Institute for Synthetic Biomedicine Helmholtz Zentrum München

Ingolstaedter Landstr. 1, 85764 Oberschleissheim, Germany

M. V. Efremova, J. Francke, R. Lavrijsen
Department of Applied Physics and Science Education

Eindhoven University of Technology PO Box 513, Eindhoven 5600 MB, The Netherlands

U. Wiedwald, R. Meckenstock, N. Josten, M. Farle Faculty of Physics and Center for Nanointegration (CENIDE) Duisburg-Essen

University of Duisburg-Essen

Lotharstraße 1, 47057 Duisburg, Germany

Adv. Funct. Mater. 2025, 35, 2418013 2418013 (1 of 18)

© 2025 The Author(s). Advanced Functional Materials published by Wiley-VCH Gmb

www.advancedsciencenews.com

www.afm-journal.d

ferritin cage is small (\$\approx 8\$ nm), holding only \$\approx 4000\$ Fe atoms, \$\begin{small} 15 \\ 15 \end{small}\$ nanocompartment from Myxococcus xanthus in mammalian cell

and is highly conserved, allowing for little modifications by bioengineering. $^{[16,17]}$ Li et al. coupled ferritin to micrometerlong Inkabox-PAK4 scaffolds, which enabled magnetic manipulation but only after iron-loading in vitro followed by cell uptake. $^{[18]}$ Another way to overcome the limitations of native ferritin is its reconstitution with magnetite Fe_3O_4 , cobalt ferrite $CoFe_2O_4$, and other ferri/ferromagnetic iron oxide species ("magnetoferritin"), $^{[19-21]}$ but this is not possible in live cells.

A promising strategy for working with live cells is thus to identify genetically controlled nanocompartments that can facilitate the biomineralization of larger quantities of Fe oxides under local reaction conditions that can be tailored by bioengineering structural and enzymatic activities within the nanocompartment. This approach could enable the production of Fe biominerals with enhanced magnetic properties under physiological conditions for mammalian cells. We have previously shown that heterologous expression of an iron-biomineralizing encapsulin

H. Ohldag, T. Feggeler Advanced Light Source Lawrence Berkeley National Laboratory 6 Cyclotron Rd, Berkeley, CA 94720, USA H. Ohldag Department of Material Sciences and Engineering Stanford University 496 Lomita Mall, Stanford, CA, USA H. Ohldag Department of Physics University of California Santa Cruz 1156 High Street, Santa Cruz, CA 95064, USA T. Feggeler Department of Physics University of California Berkeley 366 Le Conte Hall, Berkeley, CA 94720, USA I. Beer, N. P. Ivleva Chair of Analytical Chemistry and Water Chemistry Institute of Water Chemistry Department of Chemistry TUM School of Natural Sciences Technical University of Munich Lichtenbergstraße 4, 85748 Garching, Germany I. B. Alieva A.N. Belozersky Institute of Physical and Chemical Biology Lomonosov Moscow State University Leninskiye Gory 1, building 40, Moscow 119234, Russian Federation A. S. Garanina, M. A. Abakumov National University of Science and Technology «MISIS» Leninskiy Prospekt 4, Moscow 119049, Russian Federation A. S. Semkina, M. A. Abakumov Department of Medical Nanobiotechnology Russian National Research Medical University Ulitsa Ostrovityanova 1, Moscow 117997, Russian Federation F. Curdt, M. Winklhofer Institut für Biologie und Umweltwissenschaften Carl von Ossietzky Universität Oldenburg Ammerländer Heerstr. 114–118, 26129 Oldenburg, Germany Max Planck Institute for Intelligent Systems Heisenbergstraße 3, 70569 Stuttgart, Germany M. Winklhofer Forschungszentrum Neurosensorik Carl von Ossietzky Universität Oldenburg Carl-von-Ossietzky-Straße 9, 26129 Oldenburg, Germany

2418013 (2 of 18)

can enable retention by magnetic-activated cell sorting (MACS and detection by magnetic resonance imaging.^[22] These capa bilities are enabled by an iron biomineralization process within self-assembling encapsulin protein shells driven by an encapsulated ferroxidase.^[22,23] Nevertheless, the specific characteristic that differentiated the fraction of sorted cells from the remain der of the population were not examined.

Subsequently, we found that the encapsulin system from Quc sibacillus thermotolerans (Qt) has a larger diameter (\approx 42 nm) and can more efficiently biomineralize iron when expressed in man malian cells. [23,24] However, unlike iron-oxides from naturally occurring magnetic cells such as magnetotactic bacteria, [25,26] the biominerals formed in Qt encapsulins expressed in mammalian cells have not been characterized carefully.

In this study, we perform a detailed analysis and identification of iron oxide-filled *Qt* encapsulins expressed in MACS-retained cells with respect to their magnetic properties, subcellular distribution, ultrastructure, and chemical composition and show how these material properties can be used to pattern cell growth.

2. Results

2.1. Mammalian Overexpression of Iron-Accumulating Encapsulins

We first generated a construct that allows expression of the selassembling encapsulin monomer from Q. thermotolerans witl a FLAG tag (QtEncFLAG) and the corresponding ferroxidase (QtIMEF) via a 2A peptide. We also co-expressed the red fluores cent protein mScarlet-I via an internal ribosome entry site (IRES for facile detection (Table S1, Supporting Information). Cellula uptake of ferrous iron was enhanced by co-expression of the iron importer Zip14FLAG (Figure 1A). After transient expression of th constructs for 24 h, ferrous ammonium sulfate was added to th medium for 48 h before cells were sorted on commercial MAC columns into "MACS-separated"; or "; MACS-retained" cells an "flow-through" cells that were not retained in the column. Th cell fraction expressing all proteins listed above but not subjected to sorting will be further referred to as non-sorted cells. Addition ally, we had a control population of HEK293T cells transfecte with a plasmid encoding mScarlet-I protein and IRES only, whic will be referred to as "no encapsulins" condition.

2.2. MACS of Encapsulin-Expressing Cells

A fraction of cells (1.77 \pm 0.41%, mean \pm SD, n=6 independen experiments) expressing the encapsulin shell, ferroxidase, and the iron importer Zip14 were reliably retained on the magnetic sorting column when placed in the magnetic field (Figure 1B). However, when the same material was passed over the sorting column outside the magnetic field, only $0.20 \pm 0.14\%$ (mean \pm SD) of cells were retained (p=0.0022, Mann-Whitney test).

In a control experiment (Figure S1, Supporting Information), we expressed the QtEnc^{FLAG} protein as an individual plas mid and replaced the DNA encoding QtIMEF or both QtIME and Zip14^{FLAG} with sequences coding for fluorescent proteins (mEos4b targeted to the encapsulin lumen (DD-mEos4b QtSig),^[22] and eYFP, respectively). In these control conditions

© 2025 The Author(s). Advanced Functional Materials published by Wiley-VCH Gmbl

www.advancedsciencenews.com

Adv. Funct. Mater. 2025, 35, 2418013

www.afm-journal.c

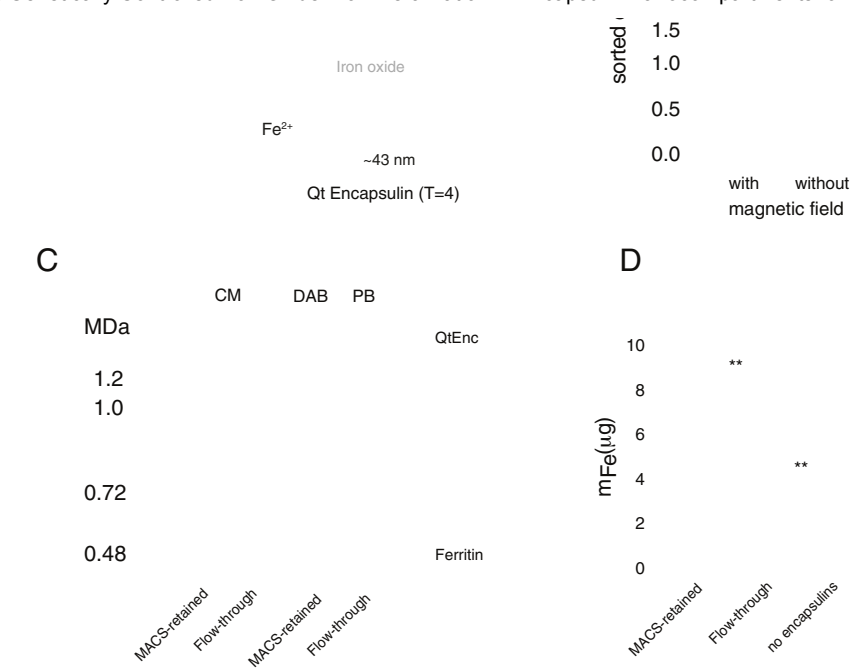


Figure 1. Magnetic-activated cell sorting of mammalian cells overexpressing iron-accumulating encapsulins. A) Scheme showing the bicistronic expresion construct encoding the ferroxidase (IMEF) from *Q. thermotolerans* (QtIMEF) together with the FLAG-tagged encapsulin monomer (via P2A), whis self-assembles into the protein shell (QtEncFLAG), and the red fluorescent protein mScarlet-I (via an IRES site). The iron transporter Zip14FLAG was c expressed from a separate plasmid, and transfected HEK293T cells were cultivated in the medium supplemented with 2 mM ferrous ammonium sulfa (FAS) for 24 h. B) Comparison of the magnetic sorting efficacy of HEK293T cells expressing QtEncFLAG with the ferroxidase IMEF and the iron transport Zip14FLAG in the commercial columns for magnetic-activated cell sorting (MACS) with or without applying a magnetic field to control for merely mecha ical retention on the columns. The cell medium was supplemented with 2 mM FAS for 24 h. Combining the expression of the above-mentioned protein and applying a magnetic field allowed for the isolation of 1.77 ± 0.41% (mean values ± SD) of the whole HEK293T cell population. Without applying magnetic field, the sorting efficiency was 0.20 ± 0.14% (mean values ± SD). Data points represent n = 6 independent transfections and experimen for each data set. Statistical analysis was performed by the Mann-Whitney test (*** corresponds to p-value < 0.01). C) Coomassie-stained Blue Native PAGE (CM) and DAB-enhanced Prussian blue-stained (DAB PB) gels loaded with whole lysates of either MACS-retained cells or flow-through cells (4.65•10⁵ cells each) showing the band of the native QtEncFLAG protein and ferritin. D) The mass of Fe contained in the pellets of MACS-retained cell flow-through cells, and control wild-type cells supplemented with 2 mM FAS (7.4 × 10⁶ cells each) was determined by inductively coupled plasma ma to p-value < 0.01). Insets show photographs of the cell pellets in test tubes after the magnetic sorting. The red color of the pellets is

only 0.13 \pm 0.20% and 0.12 \pm 0.11% were retained in the magnetic field. A statistically significant difference (p=0.0047 and p=0.0182, respectively, n=6, Kruskal-Wallis test with Dunn's multiple comparisons) was found with respect to 1.37 \pm 0.20% cells expressing QtEnc^{FLAG}, QtIMEF, and Zip14^{FLAG} (Figure S1, Supporting Information) sorted in the magnetic field.

Whole-cell lysates of MACS-retained and flow-through cells were then loaded in identical volumes onto native gels stained with either Coomassie (CM) or iron-selective Prussian bla (PB), which can be enhanced with diaminobenzidine (DAB-Pl (Figure 1C). For both MACS-retained cells and flow-throug cells, a band running above the highest marker band was vis ble by CM, consistent with the presumed molecular weight fully assembled QtEncFLAG nanocompartments (≈9.6 MDa). TI CM band and DAB PB signal for QtEnc were stronger in the MACS-separated cells. However, a DAB PB band for endogenous

Adv. Funct. Mater. 2025, 35, 2418013

2418013 (3 of 18)

© 2025 The Author(s). Advanced Functional Materials published by Wiley-VCH Gmb

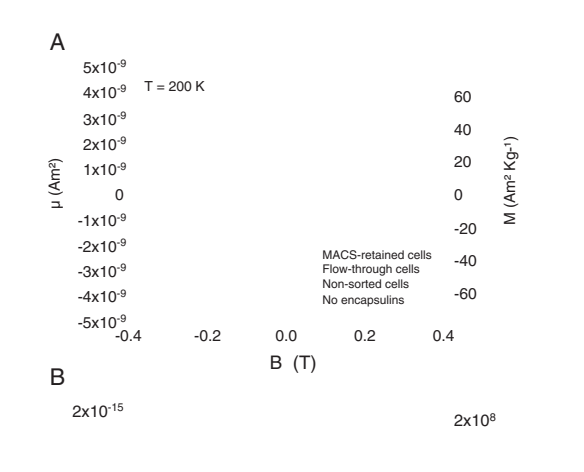
www.advancedsciencenews.com

ferritin (≈0.5 MDa molecular weight) was detectable only in flow-through cells and not in MACS-separated cells, while the CM signals were similar.

Next, we determined the cellular iron content using ICP-MS (Figure 1D). We observed an almost 3-fold increase in iron content of MACS-separated versus flow-through cells (7.29 versus 2.74 $\mu_{\rm GFe}$ per equal number of cells, $p=0.0014,\,n=3$, unpaired ttest), which still had a substantially elevated amount of iron compared to non-transfected cells (0.69 $\mu_{\rm GFe},\,p=0.0015,\,n=3$, unpaired t-test). The MACS-separated cell pellet was also more intensely stained red by the co-expressed m-Scarlet, indicating that magnetic sorting selects for highly overexpressing cells.

We tested for a possible cytotoxic effect of QtEncFLAG, QtIMEF, and Zip14FLAG expression and iron biomineralization using the LDH-Glo assay, which measures the release of lactate dehydrogenase (LDH) into the culture medium as a proxy for cell membrane damage. The analysis showed no significant difference in

www.afm-journal.d



cell viability between 0–1.5 mM FAS (p-values > 0.05, Kruskal-Wallis test with Dunn's multiple comparisons), but there was a small decrease in cell viability to 90.1 \pm 7.6% for 2 mM FAS (p=0.0448, n=6, Kruskal-Wallis test with Dunn's multiple comparisons, Figure S2, Supporting Information).

2.3. Magnetic Characterization

We applied field-dependent vibrating sample magnetometry (VSM) and ferromagnetic resonance/electron paramagnetic resonance (FMR/EPR) to quantify the magnetic properties of MACS-separated cells in comparison to flow-through cells, nonsorted cells, and cells that only expressed the fluorescent protein mScarlet-I ("no encapsulins").

We first obtained magnetic hysteresis loops of the MACS-separated cells (batch 1) at T = 200 K after cooling in a zero field and compared them with three controls (**Figure 2A**).

Diamagnetic and paramagnetic background contributions were removed, as described in the Materials & Methods section. Only the cells separated by MACS exhibited a magnetic hysteresis loop with a total sample saturation magnetic moment of $\approx\!4.0\times10^{-9}$ A m². This value is more than four times higher than the established detection limit, as evidenced by three additional samples showing magnetic responses at the noise level (1.0 \times 10^{-9} A m²). The right y-axis in Figure 2A expresses the normalized magnetic moment per amount of Fe in the ferrimagnetic state, as described below in the detailed analysis of the magnetic response by FMR. We determined a saturation magnetization $M_s=56.0~{\rm A~m^2~kg^{-1}}.$

Two exemplary hysteresis loops of the MACS-separated cells (batch 1) at T=50~K and T=200~K (Figure 2B) reflect the decreasing magnetization with temperature. The magnetization per magnetically sorted cell at 200 K is $\approx 1 \times 10^8~\mu_{\rm B}$ (right scale). It is important to note that slight asymmetries are due to the small ferrimagnetic signal overlaid with additional paramagnetic and diamagnetic signals. This becomes clearer by examining the sample response after subtracting the high-field diamagnetic susceptibility $\chi_{\rm HF}$ in Figure S3, Supporting Information. We obtain a strong and saturated paramagnetic signal ($\mu=2.8\times 10^{-7}~A~m^2$) at T=3~K and B=5~T (Figure S3A, Supporting Information), which is almost 2 orders of magnitude larger than the fer-

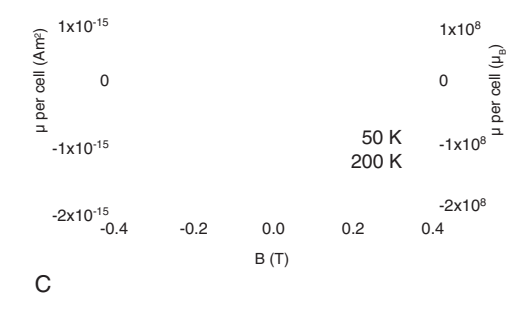


Figure 2. Vibrating sample magnetometry (VSM) and ferromagnetic resonance (FMR). A) VSM at T=200 K showing hysteresis loops of the pelets comprising $\approx 4 \times 10^6$ HEK293T cells co-expressing the QtEnc^{ELAC} QtIMEF, mScarlet-I, and Zip14^{FLAG} from MACS-retained, flow-through and non-sorted cell fractions as well as from HEK293T cells expressin the fluorescent protein mScarlet-I ("no encapsulins" condition). The cemedium was supplemented with 2 mM FAS for 48 h. The scale on the right applies to MACS-retained cells only. B) Magnetic moment per cell at T=50 K and 200 K after zero-field cooling. C) Angular-dependent FMR a 9.412 GHz and T=200 K after field cooling in B = 1 T at $\Phi=0^\circ$ from the liquid state. The green dashed curve indicates an angular-dependent FM with uniaxial anisotropy.

rimagnetic response in Figure 2A, and decays strongly with terr perature. Above $T=50~\rm K$, this Langevin paramagnetism gives strictly linear background as a function of external field on to of the ferrimagnetism, indicating that the encapsulin nanopaticles exhibit both para- and ferrimagnetic responses, and th temperature range from $50-200~\rm K$ is the best window to extrac

Adv. Funct. Mater. 2025, 35, 2418013

2418013 (4 of 18)

© 2025 The Author(s). Advanced Functional Materials published by Wiley-VCH Gmbł

www.advancedsciencenews.com

cell area of 1 \pm 2% (p < 0.001, n = 92, Dunn's multiple compa

ison after Kruskal-Wallis test).

www.afm-iournal.c

information about long-range ferrimagnetic order in the encapsulin nanoparticles. The high-field susceptibility $\chi_{\rm HF}$ decreases from $\approx \! 3.0 \times 10^{-8}$ m³ $g_{\rm Fe}^{-1}$ (2.4 \times 10 $^{-3}$ emu $g_{\rm Fe}^{-1}$ Oe $^{-1}$) at 3K to 2.5 \times 10 $^{-8}$ •m³ $g_{\rm Fe}^{-1}$ (2.0 \times 10 $^{-4}$ emu $g_{\rm Fe}^{-1}$ Oe $^{-1}$) at 200 K (Figure S3B, Supporting Information, data shown after removal of diamagnetism from the cell matrix and water). For better comparison with the literature, we give $\chi_{\rm HF}$ in SI and cgs units here.

Additionally, we assessed the reproducibility of the magnetic responses on a separate cell sample produced six months after the one presented in Figure 2A,B. We obtained highly comparable hysteresis curves at $T=200\,\mathrm{K}$ from two distinct sample batches (Figure S3C, Supporting Information).

For further proof of long-range magnetic order, we employed temperature- and angular-dependent FMR on the same sample, which was cooled down from 300 to 50 K in B = 1 T at an angle $\Phi=0^\circ$. FMR/EPR measurement at T=200 K and T=50 K (Figure 2C and Figure S3D,E Supporting Information). We observed a major angular-independent EPR line at 312 mT (g-factor of 2.15) and EPR lines at B = 210 mT (g = 3.2) and B = 155 mT (g = 4.3) with much lower intensities. To highlight the more interesting ferromagnetic component visible in the angular-dependent FMR line with uniaxial anisotropy (green dashed line), we have subtracted the strong EPR references line. The resulting demagnetization field varies between B = 115 mT for $\Phi=0^\circ$ and 330 mT for $\Phi=90^\circ$. The FMR line can be identi-

To further control for potential confounding variables, we als used fluorescence-activated cell sorting (FACS), to isolate th top 2% of cells overexpressing mScarlet-I (Figure S4, Supporting Information), which contained about half of the iron oxide core found in the MACS-retained cells. However, only 2.6 \pm 8% these cores were found in aggregates. In the MACS-retains cells, we also found multiple examples of aggregates with tightly packed iron cores, which in some instances showed sub-organization in a chain- or rod-like alignment (Figure 3I We measured the diameter of the iron-oxide cores to be 31 3 nm and the outer diameter of empty encapsulin protein shel as 40 ± 3 nm (light blue outlines in Figure 3E), in line wi cryo-TEM data we reported earlier and maximum filling of th encapsulin lumen.[23] The center-to-center distance betwee adjacent cores was 43 \pm 2 nm (Figure 3F), just slightly large than the shell diameter, thus indicating close packing of tl spheres (Figure 3F). Besides the cytosolic localization, we als observed encapsulin ensembles in the endolysosomes ar autophagosomes in all three conditions (Figure S5, Supportir Information).

2.5. Crystallinity and Elemental Analysis of Encapsulin Particles

fied by the broader peak-to-peak linewidth. The amplitude of the FMR is, however, only about 5% of the main EPR line at B=312~mT and linewidth $\Delta B_{pp}=15~mT$. We fitted the FMR angular dependencies, assuming rod-like assemblies of encapsulin nanoparticles or their preformed aggregates before subsequent freezing (green broken lines in the color plots, cf. detailed information in the discussion section). Under the assumption that the angular dependence of the FMR line solely depends on the magnetization of the encapsulin nanoparticles and their uniaxial symmetry, we extracted a magnetization of the ferrimagnetic component of 280 kA m^{-1} at 200K with uncertainties $\approx \pm 25\%$. We used this estimate to rescale the magnetization of the hysteresis loops in Figure 2A.

2.4. Intracellular Distribution of Iron-Accumulating Encapsulins

The subcellular distribution of iron-oxide-filled encapsulins was characterized using low-magnification brightfield transmission electron microscopy (TEM). Similar to our previous work, [23] QtEncFLAG co-expressed with QtIMEF and Zip14FLAG produced strong contrast in TEM micrographs due to the electron-dense iron-rich cores inside the protein shells (Figure 3).

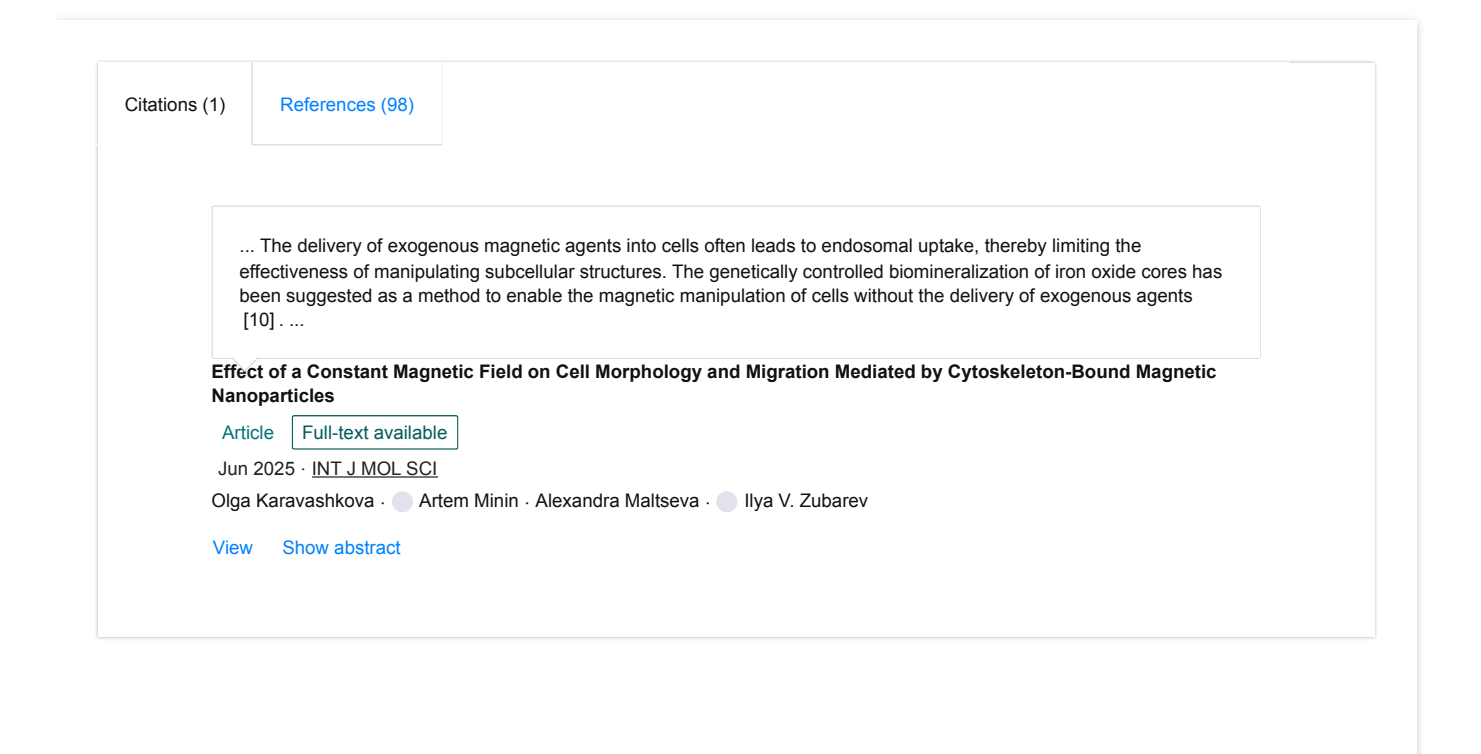
To analyze the crystalline structure of encapsulin cores in the ultrathin cell sections, we performed high-angle annular dare field (HAADF) imaging in scanning transmission electron meroscopy (STEM) mode. The HAADF-STEM image of the ecapsulin nanoparticles in MACS-separated cells (Figure 4A, demonstrates the low crystallinity of particles, i.e., the absence of long-range order, in line with the corresponding fast Fouri-Transform image (FFT image, inset) not showing any ring paterns either. Nevertheless, on the single-particle level (Figure 4C one can see that the amorphous matrix of the encapsulin core is cludes ultrafine nuclei with a short-range crystalline order (10-2 atomic columns) indicated by dark red arrows (Figure 4C, insets

According to energy-dispersive X-ray spectroscopy (EDX) ma ping, iron, phosphorus, and oxygen represent the main comp nents of encapsulin cores in MACS-separated cells (Figure 4L Analysis of the EDX linear profiles of iron and phosphori (Figure 4E,F) reveals a large variation in the average Fe:P rat from particle to particle. To check whether this ratio also depend on the agglomeration state of encapsulins, we performed a quatitative analysis of Fe and P content in 10 different areas of cel inside or outside of aggregates (insets in Figure S6A, B, Suppor ing Information). Each area contained 4–5 electron-dense enca sulin cores and was randomly chosen. We determined the Fe atomic ratio $R_{at} = 1.6\pm0.1$ (mass ratio R_{mass} of 2.9 ± 0.2) for the encapsulins in the aggregates, which was significantly high than $R_{at}=1.3{\pm}0.1$ (R $_{\rm mass}=2.4{\pm}0.2$) for the encapsulins hom geneously dispersed in the cytoplasm (p-value < 0.0001, Man Whitney test, n = 10, Figure S6C and Tables S2 and S3, Su porting Information). A center-surround pattern was discerne in some aggregated (Figure S6D, Supporting Information) ar dispersed (Figure S6E, Supporting Information) encapsulin pa ticles, with the core and shell predominantly containing iron phosphorus, respectively.

Adv. Funct. Mater. 2025, 35, 2418013

2418013 (5 of 18)

© 2025 The Author(s). Advanced Functional Materials published by Wiley-VCH Gmb



Recommended publications Discover more Article Full-text available Genetically Encoded Self-Assembling Iron Oxide Nanoparticles as a Possible Platform for Cancer-Cell... March 2021 · Pharmaceutics Mariia V. Efremova · Silviu-Vasile Bodea · Felix Sigmund · [...] · Maxim Artemovich Abakumov The study of growth and possible metastasis in animal models of tumors would benefit from reliable cell labels for noninvasive wholeorganism imaging techniques such as magnetic resonance imaging. Genetically encoded cell-tracking reporters have the advantage that they are contrast-selective for viable cells with intact protein expression machinery. Besides, these reporters do not suffer from ... [Show full abstract] View full-text Poster Ferromagnetic Resonance Spectroscopy, Micromagnetic Simulations and Scanning Transmission X-ray Micr... Thomas Feggeler · R. Meckenstock · H. Ohldag · [...] · Detlef Spoddig Read more Article An Ultrasensitive Molecular Detector for Direct Sensing of Spin Currents at Room Temperature September 2024 · ACS Applied Materials & Interfaces Thomas Feggeler · R. Meckenstock · Ulf Wiedwald · [...] · Tanja Strusch The experimental analysis of pure spin currents at interfaces is one major goal in the field of magnonics and spintronics. Complementary to the established Spin-Hall effect using the spin-to-charge conversion in heavy metals for information processing, we present a novel approach based on spin pumping detection by an interfacial, resonantly excited molecular paramagnet adsorbed to the surface of ... [Show full abstract] Read more Article Full-text available Spatially-resolved dynamic sampling of different phasic magnetic resonances of nanoparticle ensemble... April 2023 · New Journal of Physics Thomas Feggeler \cdot Johanna Lill \cdot Damian Günzing \cdot [...] \cdot H. Ohldag Nanoscaled magnetic particle ensembles are promising building blocks for realising magnon based binary logic. Element-specific realspace monitoring of magnetic resonance modes with sampling rates in the GHz regime is imperative for the experimental verification of future complex magnonic devices. Here we present the observation of different phasic magnetic resonance modes using the [Show full abstract] View full-text

Last Updated: 07 Aug 2025





Company	Support	Business solutions
About us News Careers	Help Center	Advertising Recruiting

© 2008-2025 ResearchGate GmbH. All rights reserved.

 $\mathsf{Terms} \cdot \mathsf{Privacy} \cdot \mathsf{Copyright} \cdot \mathsf{Imprint} \cdot \mathsf{Consent} \ \mathsf{preferences}$